frontiers in Earth Science

ORIGINAL RESEARCH
published: 05 January 2022
doi: 10.3389/feart.2021.786403

Depositional Models of Deep-Water Gravity-Flow in Lacustrine Basin and Its Petroleum Geological Significance—A Case Study of Chang 6 Oil Group in Heshui Area, Ordos Basin, China

Yiming Yang[1], Jun Peng[1], Zhaobing Chen[2], Xiaoying Zhou[3], Yao Zeng[1], Yubin Wang[1] and Xueying Wang[1]*

[1]School of Geoscience and Technology, Southwest Petroleum University, Chengdu, China, [2]School of Earth Sciences and Engineering, Xi'an Shiyou University, Xi'an, China, [3]Research Instituie of Petroleum Exploration and Development, Petro China Changqing Oilfield Company, Xi'an, China

Gravity-flow can carry a large number of sediments and organic matters from shallow water to deep lakes with its strong transporting energy, directly or indirectly facilitating the formation of deep-water tight reservoirs and shale reservoirs. Therefore, studying the genetic types, dynamic mechanisms, and depositional models of gravity-flow deposits is essential in the exploration of unconventional petroleum in large lacustrine basins. This research studied the genetic types, dynamic mechanisms, and sedimentary models of the gravity-flow deposits of the Chang 6 oil group in the Heshui Area, Ordos Basin, China, aiming to reveal its petroleum geological significance. Core observation, microscopic thin section identification, particle size analysis, and determination of rare earth elements were carried out. As a result, three types of gravity-flow deposits are detected, namely, slide-slump, sandy debris flow, and turbidity current. A certain slope gradient in bed form is the necessary geomorphic condition for gravity flow formation, and determines its development level, distribution range, and flow transformation efficiency. Sufficient provenance lays the material foundation and determines its depositional composition and development type. Other factors include earthquakes, volcanoes, and floods, which serve as triggering forces. In addition, fragmentation, liquefaction, and fluid mixing are the main dynamic mechanisms driving flow transformation. Based on the flow type of gravity flow, particle size characteristics, gravity-flow transformation relations, development mechanism, and spatial distribution pattern, we distinguished two depositional gravity-flow models, i.e., slump turbidite body and sublacustrine fan. Re-portrait the spatial distribution of deep-water gravity flow in the study area. From the perspective of sedimentology, explain the genesis of sand bodies in the northeast and southwest. The sandy debris flow in the middle fan braided channel microfacies of the sublacustrine fan sways the development of thick massive sand bodies in the study area. Hybrid event beds formed by the fluid transformation in a slump turbidite are the potential dessert area for deep-water tight oil and gas.

Keywords: lacustrine gravity-flow channels, unconventional petroleum, sublacustrine fans, slump olistoliths, tight sandstone reservoir

OPEN ACCESS

Edited by:
Dongdong Liu,
China University of Petroleum, China

Reviewed by:
Hexin Huang,
Chang'an University, China
Pengfei Wang,
China Geological Survey, China

****Correspondence:***
Jun Peng
pengjun@swpu.edu.cn

Specialty section:
This article was submitted to Economic Geology, a section of the journal Frontiers in Earth Science

Received: *30 September 2021*
Accepted: *29 November 2021*
Published: *05 January 2022*

Citation:
Yang Y, Peng J, Chen Z, Zhou X, Zeng Y, Wang Y and Wang X (2022) Depositional Models of Deep-Water Gravity-Flow in Lacustrine Basin and Its Petroleum Geological Significance—A Case Study of Chang 6 Oil Group in Heshui Area, Ordos Basin, China. Front. Earth Sci. 9:786403. doi: 10.3389/feart.2021.786403

1 INTRODUCTION

Sand body of deep-water gravity-flow refers to gravity-driven sands deposited in deep-water areas below the storm wave base plane, which is currently a key area for unconventional petroleum exploration (Haughton et al., 2009; Zou et al., 2009; Zou et al., 2012; Cao et al., 2017). The gravity-flow deposit is affected by various factors, including the lake basin bottom shape, provenance supply, tectonic activity, and climate, which means that gravity-flow itself is a key indicator of paleotectonic movement, paleo-source input, and paleoclimatic evolution (Amy et al., 2005; Ma et al., 2017; Yang et al., 2020). Gravity-flow transports huge amounts of deposits from shallow to deep water of the lake basin, forming a favorable space for the transportation, aggregation, and preservation of oil and gas resources (Fic and Pedersen, 2013; Ghanizadeh et al., 2015; Li X. et al., 2018; Wang et al., 2018). In addition, a large amount of organic matter is also carried during the process, promoting hydrocarbon generation and expulsion from the mud shale at the bottom of the lake (Stevenson and Peakall, 2010; Bernhardt et al., 2012). Thus, gravity-flow is closely related to the forming of the deep-water tight reservoir and argillaceous shale reservoir (Zou et al., 2012; Yang and Deng, 2013; Yang et al., 2014; Bell et al., 2018). The study on gravity-flow was initiated from the turbidity current theory proposed in 1950 (Kuenen and Migliorini, 1950). The deep-water gravity-flow deposits formed by the re-transport of marine sediments have been taken as the main research object by later 54 generations (Bouma, 1962; Lowe, 1982; Shanmugam, 1997; Shanmugam, 2000; Mchargue et al., 2011; Shanmugam, 2013; Covault et al., 2014; Shanmugam, 2016; Xu et al., 2016), but the study on lacustrine gravity-flow has been neglected. In recent years, based on the research of marine deep-water gravity flow, great progress has been made in the studies on deep-water gravity-flow in terrestrial lake basins (Yang et al., 2014; Sonnenberg, 2017; Kvale et al., 2017; Pan et al., 2017; Perry et al., 2017; Wang et al., 2018). The genetic types, dynamic mechanisms, and sedimentary gravity-flow models have become the focus in petroleum geology (Mulder and Alexander, 2001, Mulder, 2009; Talling et al., 2012a, 2012b). As research unfolds, multiple geneses of deep-water deposits are recognized. The multi-solution nature and complexity of deep-water sedimentation patterns also become more prominent for lacustrine basin with frequent lake level rise and fall, multiple provenances, and instability (Shanmugan, 2000; Qiao et al., 2013; Pu et al., 2014; Du, 2015 ; Ran and Zhou., 2019). Overall, better understandings of the genetic types, dynamic mechanisms, and depositional models of gravity-flow are conducive to deep-water oil and gas exploration.

The Chang 7 and Chang 6 members of the Yanchang Formation in the Ordos Basin in central China are typical sections of gravity-flow deposits and the key targets for deep-water tight oil and gas reservoirs exploration. Chang 7 oil group in the Jiyuan area is a lithologic reservoir controlled by a large-scale turbidity current discovered earlier (Fu et al., 2008; Zou et al., 2009; Zhang et al., 2016). Then, large areas of deep-water oil-bearing sandstones in Chang 6 oil group in Bai Bao and Huaqing areas were discovered (Zhao et al., 2008; Li et al., 2009; Liu et al., 2015), further expanding the exploration field of the deep-water tight reservoir. Extensive studies have been conducted on the provenance, paleontology, and geochemical characteristics of gravity-flow deposits in Chang 7 and Chang 6 (Luo et al., 2007; Yang and Deng., 2013; Yao et al., 2013; Zhang et al., 2014; Yuan et al., 2015; Fu et al., 2018). However, no universal cognition on the depositional models of gravity-flow has been made, with a single sedimentary model being used in the previous research to explain these deposits in this area (Yang et al., 2014; Zhang et al., 2016; Liu et al., 2017). Most works studied the characteristics of gravity-flow deposits by taking slide-slump, sandy debris flow, and turbidity current as research objects without considering the macroscopic depositional context or depositional patterns (Fu et al., 2008; Li et al., 2011; Zou et al., 2012; Ran and Zhou., 2019). However, we believe that ultra-thick tight sand bodies in deep water are derived from the superposition of multi-phase, multiple, and multi-modal gravity flow, while the models of gravity-flow deposits involve various factors, including flow type, flow transformation relation, and genesis mechanism. Given the diverse sedimentological characteristics of the same deposits in different depositional models, a reasonable and complete correlation model should be established for the facies and deposition modes, which are the foundations for the study on late reservoir and accumulation, etc. The methods only considering flow types are inappropriate, so are the approaches using a single depositional model to explain the gravity-flow deposits of complex genesis.

Based on numerous core observations and comprehensive geological studies, the Chang 6 oil group in the Heshui area of Ordos Basin is taken as a case area to investigate the models of gravity-flow deposits. Sedimentological characteristics are adopted as the reference to identify the flow types in the study area. Referring to existing research results, we elaborated the origin background, triggering mechanism, and flow transformation relationship of gravity-flow deposits based on lithological signatures. Depositional facies, subfacies, and microfacies are also distinguished to establish deposition models of gravity flow. Re-describe the spatial distribution characteristics of deep-water gravity flow in the study area. From the perspective of sedimentology, the genesis of different sand bodies are revealed. It is hoped that by deepening the understanding of the gravity-flow system of semi-deep and deep lacustrine basins, and by establishing a detailed geological model, the exploration and development of unconventional petroleum such as deep-water tight sandstones and mud shales can have clearer guidance.

2 GEOLOGICAL SETTINGS

2.1 Tectonic Characteristics

The Heshui area is an important oil-generating area located in the southwest of the Ordos Basin, which is located in Qingcheng and Heshui County, Gansu Province, adjacent to Qingyang in the west,

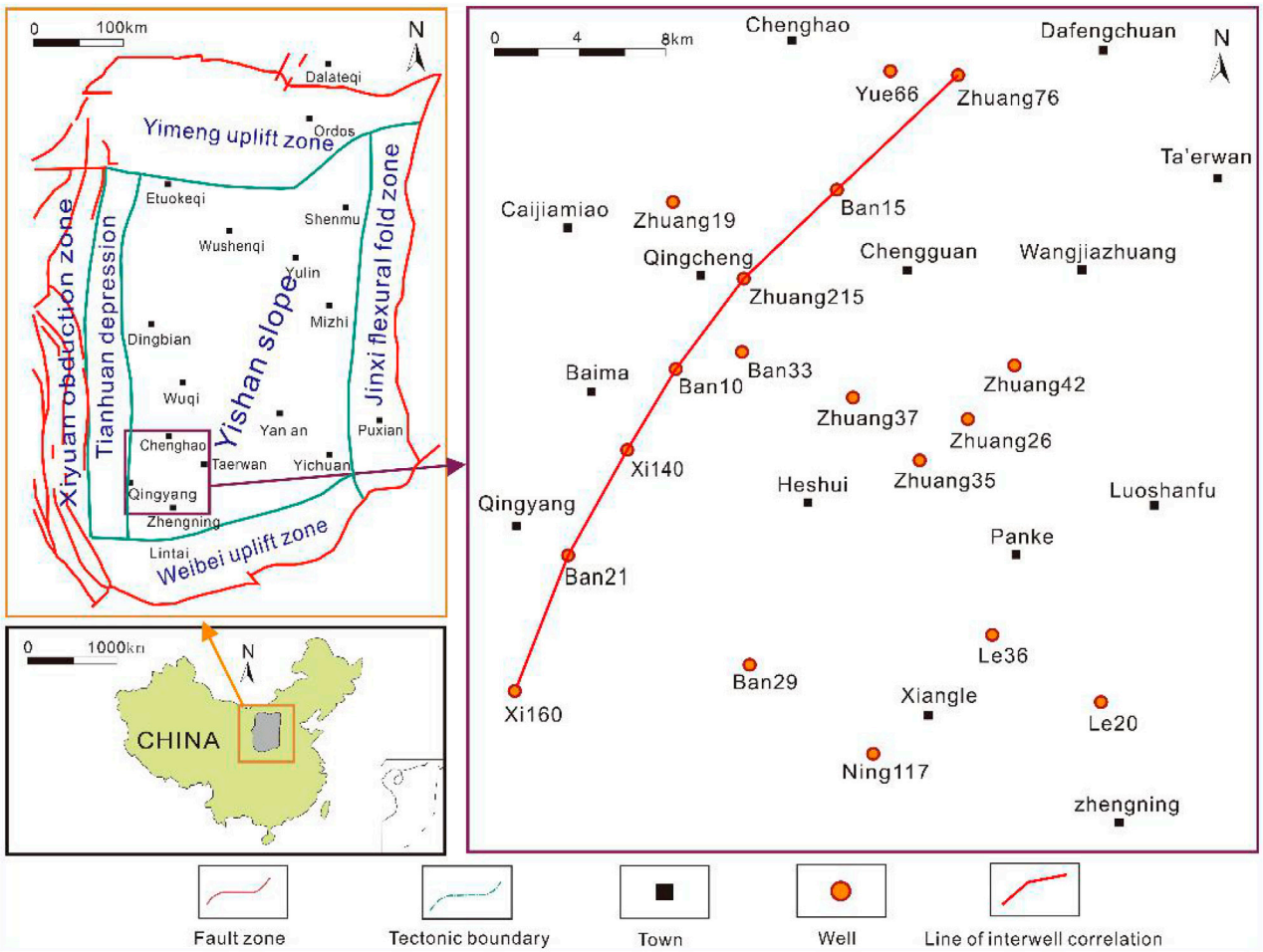

FIGURE 1 | Tectonic division of Ordos Basin and the location of the study area, connecting-well profiles, wells in this study, and the wells sampled therein.

Ta'erwan in the east, Chenghao in the north, and Ning County in the south, with an exploration area of about 750 km^2. It is tectonically located in a tectonic depression in the middle part of the Yi-Shaan Slope in Ordos Basin, which is at the intersection center of multiple depositional systems of Yanchang Formation in Ordos Basin, and local small nose-shaped uplift is developed (**Figure 1**). The Chang 6 oil reservoir group is gravity-flow deposits of various types developed in the context of the semi-deep and deep lake (Liu et al., 2015; Xu et al., 2016; Li X. et al., 2018; Ran and Zhou., 2019) during a special period of return uplift after the maximum expansion period of Chang 7 Lake Basin (**Figure 2**). It has been an important exploration section for unconventional petroleum such as deep-water tight sandstone reservoirs and mud shale reservoirs in Ordos Basin in recent years.

2.2 Depositional and Stratum Characteristics

As the subsidence center of the Ordos Basin during the Yanchang period, the Heshui area inherited the same sedimentary and stratum characteristics as the Ordos Basin. The Ordos Basin, a craton foreland basin located on the North China Plain, is characterized by a stable basement, multi-phase fault depression, obvious migration oscillation, and multi-phase cycle superposition (Zhang, 1989; He, 2003; Yu et al., 2010). During the Triassic period, the thrust and nappe of the North Qinling led to the rapid expansion of the base plane and the deepening of water. Due to the influence of the Indochina movement in the Late Triassic period, the Ordos Basin gradually transformed from marine to lacustrine basin deposits and developed a set of lacustrine terrigenous clastic rocks with a thickness of about 1,300 m, that is, the Yanchang Formation. The bottom of the Yanchang Formation is relatively flat, and the denudation at the top varies greatly. The Yanchang Formation is in pseudo-integrated contact with the overlying Yan'an Formation or Fuxian Formation (He, 2003; Li Z. et al., 2018; Xian et al., 2018). From top to bottom, the Yanchang Formation can be divided into ten oil reservoir sections covering Chang 1 to Chang 10. The features of depositional evolution reflect the entire

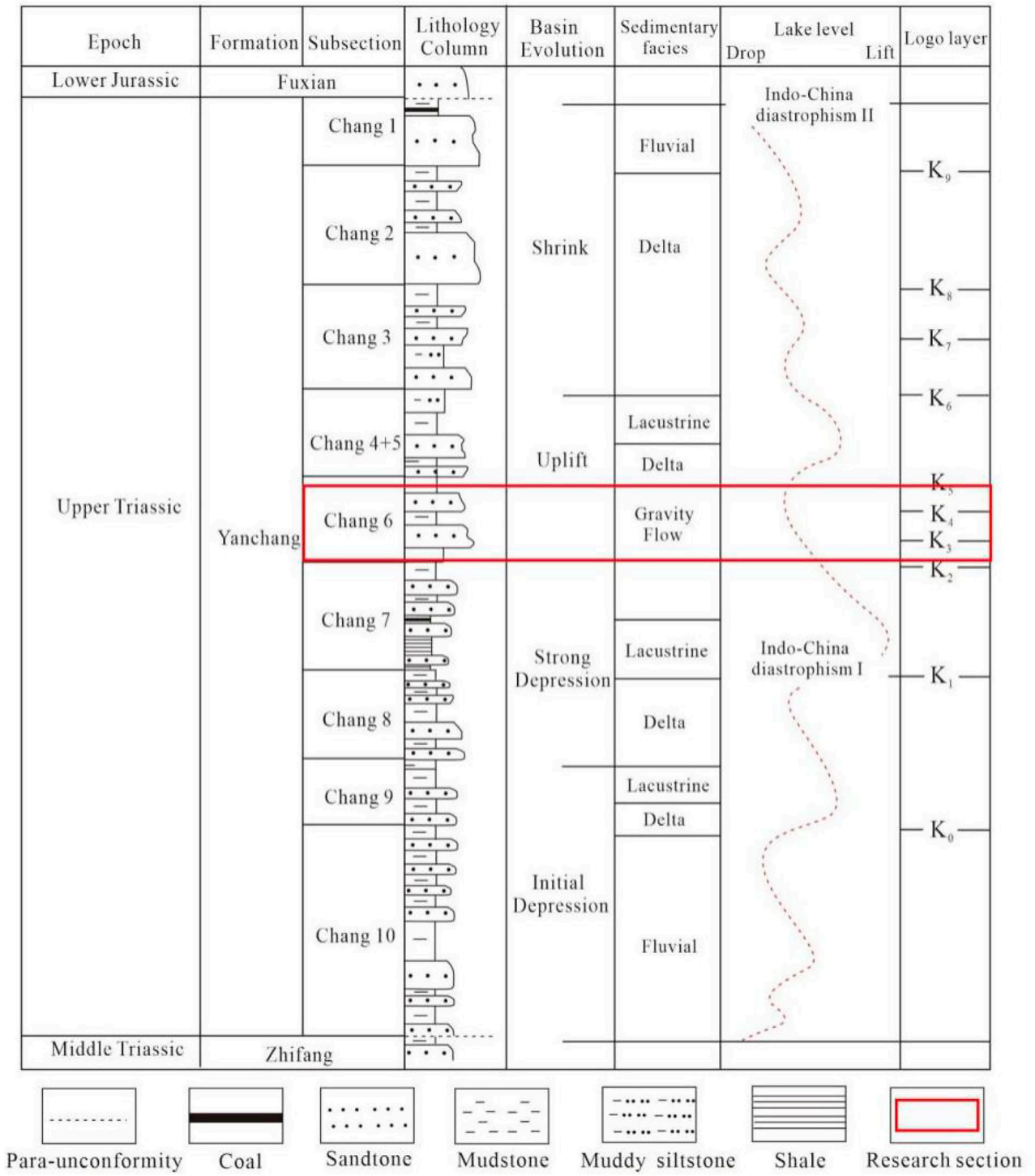

FIGURE 2 | Histogram of sedimentary evolution of the Yanchang Formation (histogram of sedimentary evolution of the Yanchang Formation from Ran et al., 2019).

formation and extinction processes of lake basins, during which a variety of depositional systems such as alluvial fans, rivers, deltas, and lakes were developed (**Figure 2**). The deep-water gravity-flow deposits of Chang 6 in the Heshui area can be regarded as an underwater extension system deposited in the semi-deep and deep lake. It is formed by front deposits of the large-scale prograded delta, which migrated to the center of the lake basin and collapsed under the action of flood, earthquake, and volcano (Li et al., 2009; Zou et al., 2012; Li X. et al., 2018).

TABLE 1 | The number, well name, formation, subsection, and depth range of wells used in the core observation and description. See **Figure 1** for the location of wells.

Number	Well	Formation	Subsection	Depth range/m
1	Le36	Yanchang	Chang 6	1,242.4–1,370.0
2	Zhen65	Yanchang	Chang 6	1,304.3–1,411.7
3	Ban33	Yanchang	Chang 6	1,729.0–1,850.0
4	Le20	Yanchang	Chang 6	1,430.0–1,536.0
5	Ling96	Yanchang	Chang 6	1,588.9–1,678.7
6	Yue66	Yanchang	Chang 6	1,903.9–2,028.0
7	Li54	Yanchang	Chang 6	1,775.5–1,804.1
8	Bai246 (Neighbor area)	Yanchang	Chang 6	1,800.0–1,896.9
9	Ling79 (Neighbor area)	Yanchang	Chang 6	1,950.2–2,003.3
10	Zhuang42	Yanchang	Chang 6	1,711.0–1,820.0
11	Ban29	Yanchang	Chang 6	1,403.0–1,520.8

TABLE 2 | The number, well name, formation, subsection, and depth range of samples used in the fragment composition analysis and heavy mineral composition analysis under the microscope. See **Figure 1** for the location of wells.

Number	Well	Formation	Subsection	Number	Depth range of samples/m
1	Zhuang35	Yanchang	Chang 6	10	1,693.0–1,793.9
2	Zhuang37	Yanchang	Chang 6	14	1,606.0–1,708.5
3	Zhuang26	Yanchang	Chang 6	9	1,690.0–1,810.0
4	Zhuang19	Yanchang	Chang 6	11	1,856.5–1,966.6
5	Ning142	Yanchang	Chang 6	10	1,562.0–1,670.0
6	Ning25	Yanchang	Chang 6	8	1,298.0–1,412.3
7	Ning146	Yanchang	Chang 6	12	1,578.0–1,695.3
8	Ning117	Yanchang	Chang 6	8	1,399.0–1,516.1

3 SAMPLES, EXPERIMENTS, AND DATA SOURCES

A total of 11 core wells were observed in this study, among which well Zhuang 42 and well Ban 29 are detailed (**Table 1**).

A total of 82 sandstone samples from Chang 6 oil group of Zhuang 35, Zhuang 37, Zhuang 26, Zhuang 19, Ning 142, Ning 25, Ning 146, and Ning 117 wells (see **Figure 2** for the location of wells) were collected for microscopic thin section identification. The samples were all ground in thin sections at Xi'an Shiyou University. Microscopic observation, photography, and mineral statistics were conducted on the polished rock thin sections. Related work was carried out under a Leica ICC50 HD microscope. Eight areas were randomly selected from each thin section for rock mineral statistics, and the sandstone mineral areas were drawn in CorelDraw X16 and filled with different colors. Color pixel counts were completed with Photoshop software, and the content of quartz, feldspar, rock debris, and heavy minerals was classified (**Table 2**).

The Malvern MS-3000 laser particle size analyzer was adopted to analyze the particle size of 62 sandstone samples from Chang 6 oil group of Zhuang 35, Zhuang 37, Zhuang 26, Zhuang 12, and Ban 29 wells. The C and M values obtained from the analyses were cast into the C-M plate to draw an average line parallel to the C = M baseline in the sample point group. The Im value represents the horizontal distance between the average line and the C = M baseline. The smaller the Im value, the smaller the difference between the maximum hydrodynamic force and the average hydrodynamic force, which indicates a better sortability of the samples. A cumulative analysis of the particle size probability was conducted for three typical samples at 1859.3 m of Zhang 42, 1,695.7 m of Zhang 35, and 1,654.4 m of Ban 29 (**Table 3**).

ICP-OES + MS, an inductively coupled plasma spectrometer, was employed to determine the content of rare earth elements in nine sandstone samples from Chang 6 oil reservoir group of Le 36, Ban 33, and Zhuang 37 wells, as well as 11 siltstone samples from Chang 7 oil group of Le 36, Ban 33, and Zhuang 42 wells (**Table 4**).

The particle size analysis and trace element determination experiments were completed at the State Key Laboratory of Oil and Gas Reservoir Geology and Exploration of Chengdu University of Technology.

4 RESULTS

4.1 Result of Particle Size Analysis

The samples of 1859.3 m from Zhuang 42 well, 1,695.7 m from Zhuang 35 well, and 1,654.4 m from Ban 29 well were taken. The cumulative curves of particle size probability show large suspended component with low gradient (**Figure 3A**); suspended component accounts for most of the content with a slight amount of saltation population content with the size less than 1ϕ, and low gradient (**Figure 3C**); higher saltation population content and the cut-off point between this content and the suspended component is at about 2ϕ, and the gradient is low overall (**Figure 3E**). The Im values of slide-slump rocks, sandy debris flow, and turbidity current are 3.13, 2.28, and 2.32, respectively (**Figure 3B**, **Figures 3D,F**).

4.2 Result of Heavy Mineral Identification

Thin section identification is adopted for the zonal statistics of the heavy minerals in the study area, and the results obtained are as

TABLE 3 | The number, well name, formation, subsection, and depth range of samples used in the sandstone grain size analysis. See **Figure 2** for the location of wells. See **Figure 1** for the location of wells.

Number	Well	Formation	Subsection	Number	Depth range of samples/m
1	Zhuang35	Yanchang	Chang 6	10	1,693.0–1,793.9
2	Zhuang37	Yanchang	Chang 6	7	1,606.0–1,708.5
3	Zhuang26	Yanchang	Chang 6	16	1,690.0–1,810.0
4	Zhuang42	Yanchang	Chang 6	18	1,856.5–1,966.6
5	Ban29	Yanchang	Chang 6	11	1,562.0–1,670.0

TABLE 4 | The number, well name, formation, subsection, and depth range of samples used to determine rare earth element content. See **Figure 1** for the location of wells.

Number	Well	Formation	Subsection	Number	Depth range of samples/m
1	Le36	Yanchang	Chang 6	2	1,242.4–1,370.0
2	Ban33	Yanchang	Chang 6	2	1729.0–1850.0
3	Zhuang37	Yanchang	Chang 6	3	1,606.0–1708.5
4	Zhuang42	Yanchang	Chang 6	2	1,610.0–1711.0
4	Le36	Yanchang	Chang 7	3	1,242.4–1,370.0
5	Ban33	Yanchang	Chang 7	5	1729.0–1850.0
6	Zhuang42	Yanchang	Chang 7	3	1711.0–1820.0

follows: the northeast and southwest of the study area are dominated by zircon. However, the former is observed to develop a small amount of tourmaline and garnet, while the latter a small amount of leucite and garnet. As for the central part, zircon still dominates, followed by tourmaline and garnet. A small amount of albite is also developed, showing its inheritance of the characteristics of the northeastern maternal provenance (**Table 5**). The ZTR index refers to the proportion of zircon, rutile, and tourmaline, three super-stable heavy minerals, in transparent heavy minerals.

4.3 The Determination Results of Rare Earth Elements

The determination results of rare earth elements of nine rock samples from wells Le 36, Ban 33, Zhuang 37, and Zhuang 42 reveal that the REE distribution features right gentle inclination of rich in light rare earth (LREE) and depletion in heavy rare earth (HREE), with obvious negative Eu anomaly (**Figure 4A**). La/Yb-∑REE source rock identification chart is adopted to analyze 20 sandstone samples in the study area, showing that most data points are distributed in the basaltic region and depositional rock region, and a few in the granitic region and alkaline basaltic region (**Figure 4B**).

5 DISCUSSION

5.1 Petrological Characteristics of Gravity Flow Deposits

Based on the results obtained from the core observations of several coring wells in the study area, the fluid rheological characteristics, and the methods employed to classify deep-water gravity-flow inside and outside China, we divided the gravity-flow in the study area into three main types: slide-slump featuring mass transport, sandy debris flow with plastic rheological properties, and turbidity current with Newtonian rheological characteristics.

5.1.1 Slide-Slump and the Petrological Characteristics of Its Deposits

Sliding rocks are gravity-flow deposits formed by massive deposits moving along a sliding surface without internal deformation. However, they tend to be twisted and deformed under shear stress, and then deposit in the middle and lower parts of the slope, or collapse into unconsolidated allogenic deposits, forming slump rocks with syn-sedimentary deformation structure (Shanmugam G, 2013). In view of their quick change from slide to slump and the nuance in flow, they are collectively referred to as slide-slump in this study. According to core observation, the lithology of the deposits caused by slide-slump is mainly gray-dark gray fine sandstone, siltstone, and argillaceous siltstone with mixed gravel, sand, and mud characteristics. Synsedimentary deformation structure including slump sandy folds (**Figure 5A**; **Table 6**), convolute bedding (**Figures 5B,C**; **Table 6**), sand pillow structures (**Figure 5D**; **Table 6**), iron nodules (**Figure 5E**; **Table 6**), mud tearing debris (**Figure 5F**; **Table 6**), and bedding plane structure including load casts (**Figures 5G,H**; **Table 6**) are identified. "Gravel capsules" encapsulated in sandstone or mudstone are also visible sometimes, exhibiting the characteristics of unconsolidated slide-slump deposits to erode and subsequently transport prior deposits (Chen C. et al., 2019).

5.1.2 Sandy Debris Flow and the Petrological Characteristics of Its Deposits

Sandy debris flow, a kind of gravity-flow in the plastic flow state, is layered viscous fluid and it usually deposits in a "bulk freezing" manner (Fu et al., 2010; Li et al., 2011; Mchargue et al., 2011; Shanmugan, 2013), and it has a high matrix strength. Sandy debris-flow deposits are widely developed in the study area. According to core observation, the lithology of the deposits caused by sandy debris flow is mainly massive gray-gray-black fine sandstone, siltstone, and fine siltstone. Macroscopically, granular structures (**Figures 6A,B**; **Table 7**) or blocky structures (**Figure 6C**; **Table 7**) can be seen. Laminated surfaces between multi-phase sandy debris flows can be

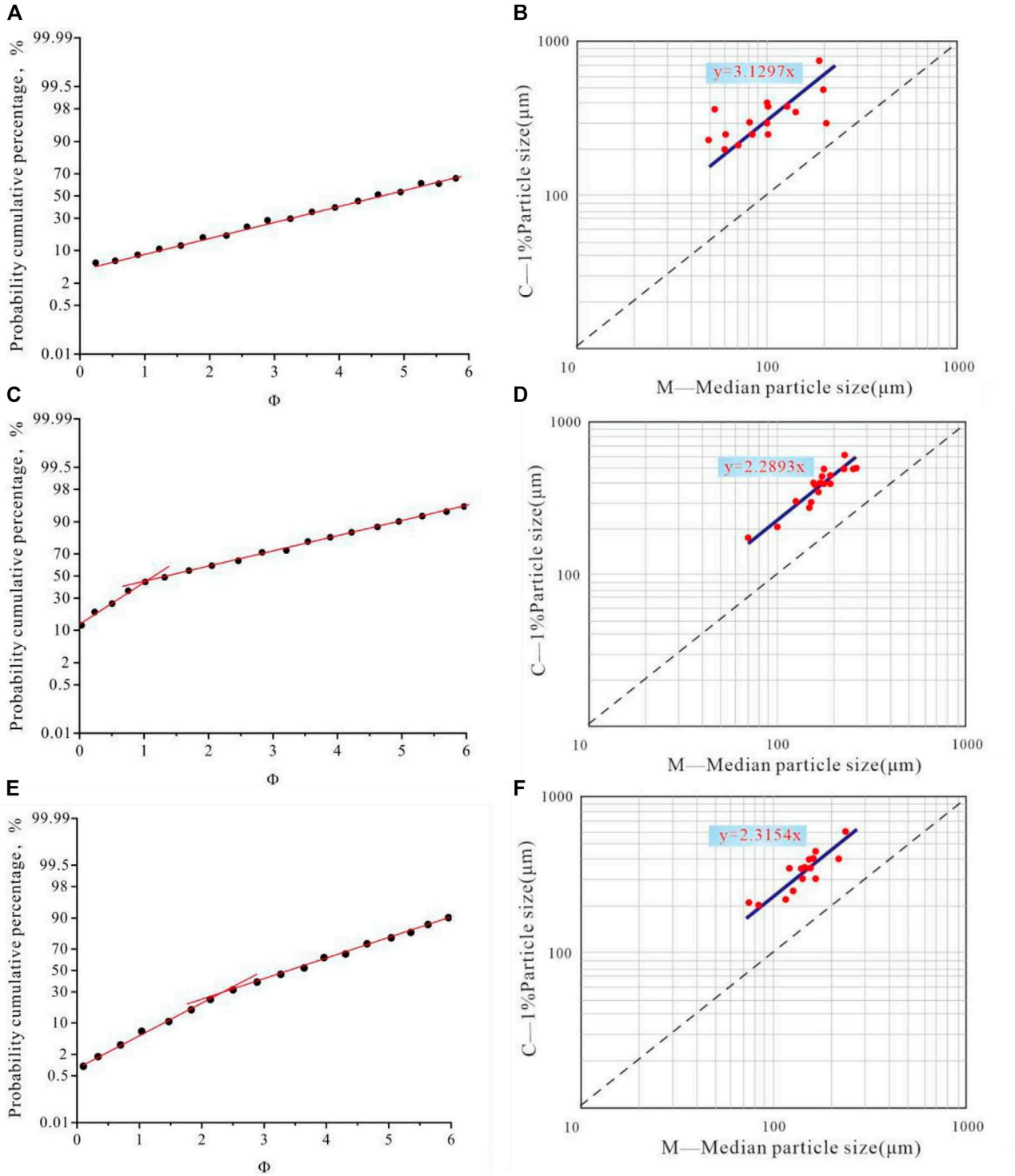

FIGURE 3 | Particle size analysis results of different gravity-flow types. **(A)** Cumulative curve of particle size probability of sandstone samples in slide-slump rocks taken from well Zhuang42, 1859.3 m; **(B)** C-M particle size distribution map of sandstone samples in slide-slump rocks; **(C)** Cumulative curve of particle size probability of sandstone samples in sandy turbidity taken from well Zhuang35, 1,695.7 m; **(D)** C-M particle size distribution map of sandstone samples in sandy turbidity current; **(E)** Cumulative curve of particle size probability of sandstone samples in turbidity taken from well Ban29, 1,654.4 m; **(F)** C-M particle size distribution map of sandstone samples in turbidity current.

TABLE 5 | Comprehensive analysis table of provenance characteristics in the study area.

Subsection	Characteristic parameters	The southwestern part of the study area	The northeastern part of the study area	The centre of the study area zircon
Chang 6	Heavy mineral composition ZTR index	Zircon (>50%) + white titanium + little garnet 0.4	zircon (>50%) +tourmaline + little garnet 0.6	(>50%) + tourmaline + garnet + little white titanium 0.6

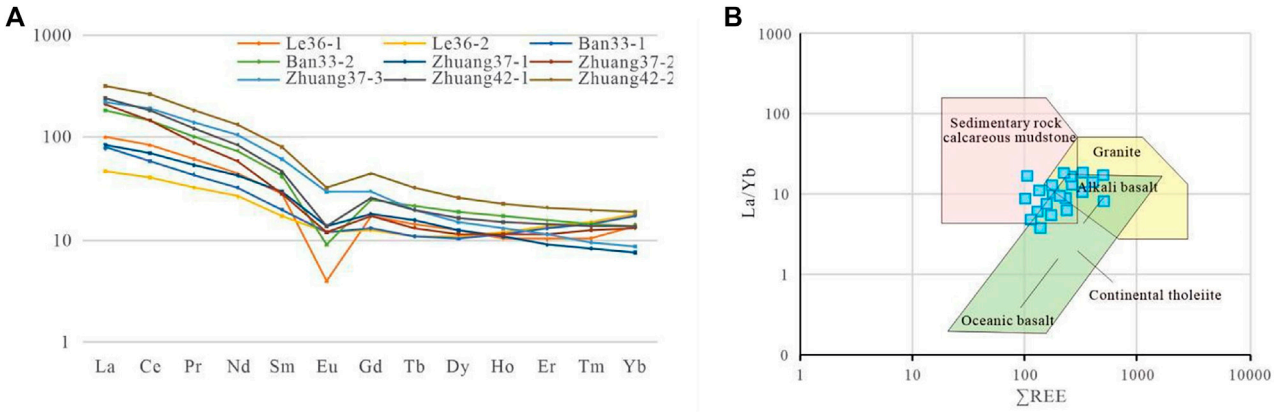

FIGURE 4 | Rare earth element analysis diagram. **(A)** The REE distribution of the sample in the research area; **(B)** La/Yb-∑REE diagram in the research area.

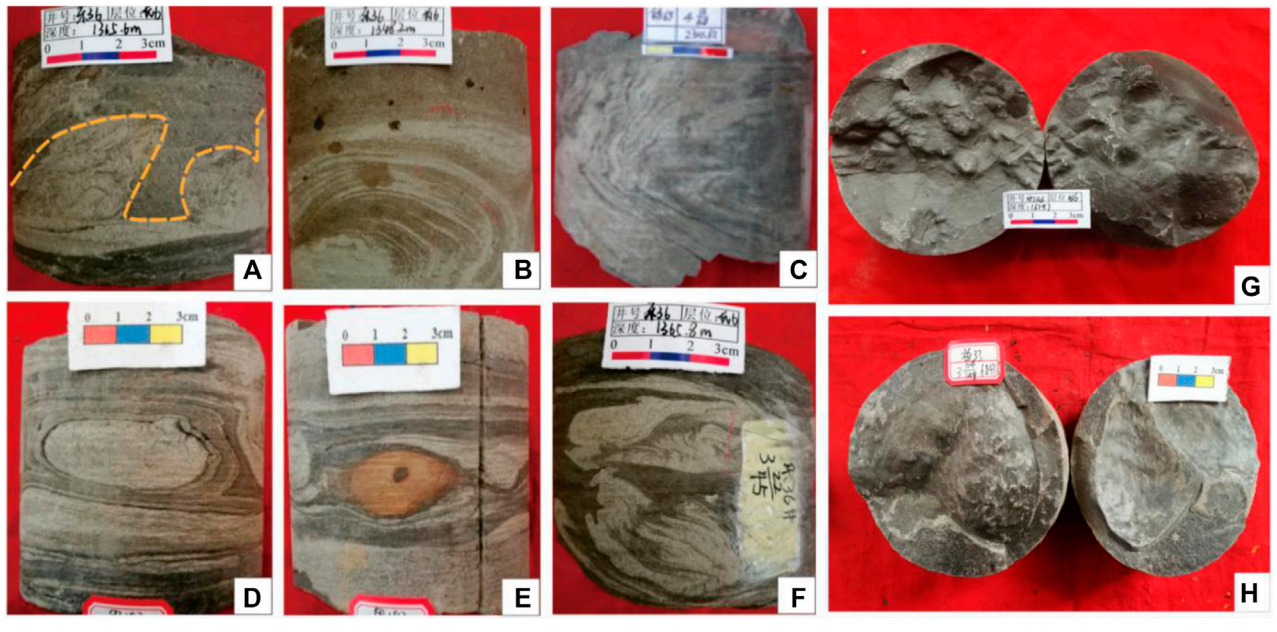

FIGURE 5 | Core depositional characteristics of slide-slump rock on core and outcropping.

found regularly, and the lithology is abrupt and irregular, showing a directional distribution of mud bands on the top of the blocky sand bodies (**Figures 6A,D,E**; **Table 7**). Sandy debris flows erode the underlying deposits to a certain extent, which is manifested in the core as a large number of irregular mud tear debris floating inside the sand body (**Figures 6F,G**; **Table 7**). In addition, scouring structures in bedding planes covering trench and groove are also commonly found (**Figures 6H,I**; **Table 7**).

TABLE 6 | The well name, depth, and phenomenon description of **Figure 5**. See **Figure 1** for the locations of wells.

Figure 3	Well name	Depth/m	Phenomenon description
A	Le 36	1,365.6–1,365.7	Slump sandy folds
B	Le 36	1,348.2–1,348.3	Convolute bedding
C	Zhen 65	2,304.6–2,304.7	Slump deformation structure, micro-deformated convolute bedding
D	Zhuang 36	1,735.76–1,735.8	Slump rocks, ball pillow structure
E	Ning 142	1,706.5–1,706.6	Slump rocks, ball pillow structure and iron nodules
F	Le 36	1,365.8–1,365.9	Mixing structure with strong slump deformation
G	Ning 146	1,679.7	Heavy load casts on bedding plane
H	Ban 33	1,847.6	Heavy load casts on bedding plane

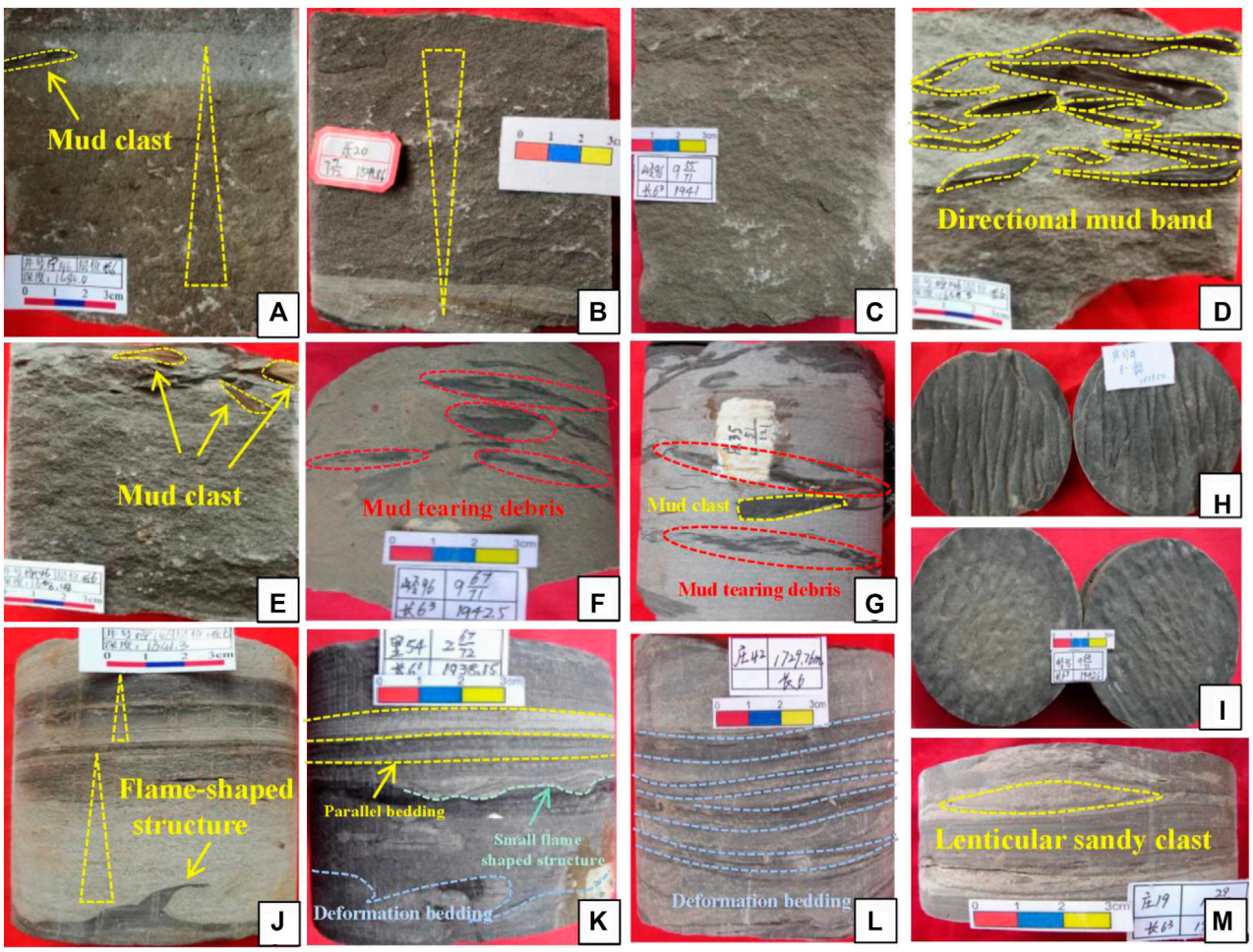

FIGURE 6 | Depositional characteristics of sandy debris flow and turbidity current on core.

5.1.3 Turbidity Flow and the Petrological Characteristics of Its Deposits

Turbidity current is a gravity-flow with fluid rheological characteristics, where particles are supported by turbulence and characterized by suspension-sedimentation (Shanmugan, 2000; Fu et al., 2008; Zou et al., 2012; Xu et al., 2016). Turbidity current deposits are widely developed in the study area and the deposits caused by turbidity shown in the cores as fine-siltstone with positive grain sequences (**Figure 6J**; **Table 6**) and less thickness. The common ones are parallel bedding (**Figure 6J**; **Table 6**), horizontal bedding (**Figure 6K**), and deformation bedding (**Figures 6K,L**; **Table 6**). Flame-shaped structures (**Figures 6J,K**; **Table 6**) are developed at the bottom. Lenticular sand bodies in the mudstone are also visible, and they boast homogeneous massive inside (**Figure 6M**; **Table 6**). Some turbidity currents are presented as incomplete Bouma sequences of AB, AC, AE sections, etc.

TABLE 7 | The well name, depth, and phenomenon description of **Figure 4**. See **Figure 1** for the locations of wells.

Figure 4	Well name	Depth/m	Phenomenon description
A	Ning 46	1,684.0–1,684.1	Blocky sand debris flow with a positive grain sequence inside and a directional mudstone at the top
B	Ling 96	1,549.8–1,549.9	Blocky sand debris flow with a negative grain sequence inside, which is in abrupt contact with the underlying rock formation
C	Ling 96	1,941.0–1,941.1	Blocky sand debris flow with uniform bedding inside
D	Ning 146	1,658.48–1,658.59	Blocky sand debris flow with a large number of directional mud band at the top and the long axis parallel to the surface
E	Ning 146	1,658.48–1,658.59	Blocky sand debris flow with directional mud clast at the top
F	Ling 96	1,942.5–1,942.6	Blocky sand debris flow with directional mud tearing debris
G	Zhuang 35	1,655.5–1,655.6	Blocky sand debris flow with mud clast and mud tearing debris inside
H	Zhuang 37	1,629.5–1,629.6	Sand debris flow with contact surface of trench structure
I	Ling 96	1,942.6–1,942.7	Sand debris flow with contact surface of groove structure
J	Ning 146	1,641.3–1,641.4	Turbidite flow with bouma sequence and flame-shaped structure at the bottom
K	Li 54	1,938.15–1,938.25	Turbidite flow with parallel bedding at the top, small flame-shaped structures, and deformation bedding at the bottom
L	Zhuang 42	1,729.8–1,729.9	Turbidite flow with deformation bedding
M	Zhuang 19	1,947.7–1,947.75	Turbidite flow with lenticular sand clast and boast internal blocky structure

5.2 Particle Size Characteristics of Different Gravity Flow Deposits

The samples of 1859.3 m from Zhuang 42 well, 1,695.7 m from Zhuang 35 well, and 1,654.4 m from Ban 29 well were taken from three typical gravity-flow types: slide-slump rocks, sandy debris flow, and turbidity current. According to particle size analysis, both slide-slump rocks and sandy debris flow have high matrix strength and rapid depositional process with the deposits mainly being transported by the suspension. However, turbidity current, which is transported by both suspension and jumping, features a tractive current. The sortability is closely related to their development mechanisms and flow transformation, in terms of which, the performance of sandy debris flow ranks first, turbidity current comes second, while slide-slump the last.

5.3 Transformation Mechanism of Different Gravity Flow

Gravity drives the gravity-flow to be transported along the slope. Flow transformation, which occurs continuously with the participation of surrounding water bodies, can lead to the spatial superposition of gravity-flow of diverse types, forming interdeposition between multiple rock types and facilitating hydrocarbon generation and storage. At the same time, the flow transformation mechanism of gravity-flow also explains the differences in particle sorting of gravity-flow of various types.

1) Transformation of slide-slump to sandy debris flow

Semi-consolidated or unconsolidated deposits that stake high up the slope contain large clasts of mud and gravel, which slide down the slope in blocks due to geological events. The high matrix strength within the blocks causes large mud clasts and gravel to collide and crush under shear stress, and then deform to form gravels of varying sizes and shapes, which are distributed randomly in the sandy matrix. The participation of surrounding water prompts liquefaction of deposits to a certain extent, with the coarser gravels preferentially unloaded and deposited at the bottom. At this point, the remaining fluid is diluted, and the overall flow regime is transformed to develop a sandy debris flow with a granular support structure.

2) Transformation from sandy debris flow to turbidity current

The concentration of sandy debris flows is higher, and the supporting matrix is formed by the dispersion pressure of inter-particle collisions, heterogeneous base support, and buoyancy. Due to the lubrication of the slope and the soft mud at the bottom of the lake basin, the coarse stream of the sandy debris carrying a small amount of coarse and gravel continues to flow and undergo transformation by the liquefaction of surrounding water. The liquefaction bumped the coarser fractions and then deposited them to the bottom of the fluid, reducing the concentration of the remaining fluid. The upper part of the stagnation point at the front end of the fluid mixes with the environmental water first, creating water circulation in a small range at the head of the sandy debris flow. During the process, the head of the sandy debris flow is the first to convert to less dense turbidity deposits, which erodes the underlying strata as it flows along the slope. Such turbidity current only stops until the new sediment involved in erosion is less than the sediment deposited. Thus, turbidity currents, though being indicative of distal deposits, are non-homogeneous within layers, and the sortability of the debris fraction is poorer than that of the sandy debris flow. The single-phase turbidity current deposits are thin and interbedded frequently with sandy clastic flows longitudinally.

5.4 Dynamic Mechanism of Gravity-Flow Deposits

5.4.1 Slope of Lake Basin Bottom Shape

According to previous studies, the lake basin of Chang 6 developed during the Late Triassic period in the Ordos Basin was deformed. The thrust and nappe of the North Qinling prompted the Heshui area to inherit the bottom shape characteristics of the southwestern part of the basin, i.e., gentle in the northeast and steep in the southwest (Yang and Deng, 2013; Yang et al., 2015). Previous research observed that, in the southwest margin of the Heshui area, a slope fold zone that is

mainly characterized by the forward fault-step type is developed (Fu et al., 2010); and this zone is distributed in the area of Qingyang-Ningxian-Zhengning, showing a northwest-southeast vertical provenance orientation. Given the slope of the compacted and underlying strata, this zone is actually 3–5° in slope and 10–20 km in width (Liu et al., 2015). As a result, a certain slope drop angle in the southwest is favorable to trigger the collapse of gravity-flow in the temporary retention area of deposits, while the wide and gentle lake basin bottom shape in the northeast extends the distance of gravity-flow transport, causing multi-stage evolution of gravity-flow and increasing the efficiency of flow transformation.

5.4.2 Supply of Provenance

The adequate supply of provenance is a key condition for gravity-flow development. Existing research reveals that the Heshui area is mainly controlled by two major provenance sources in the northeast and southwest (Luo et al., 2007; Fu et al., 2010; Liu et al., 2019). The higher the ZTR index, the more mature the heavy mineral component, indicating a greater distance from the maternal source area. The southwest direction has smaller ZTR index than the northeast, while the central part has similar index with the northeast (**Table 7**). Both the heavy mineral component and the ZTR index suggest that the northeastern source, though farther from the subsidence center, is more abundantly supplied, while the southwestern source, though closer to the subsidence center, is limited in supply.

The determination results of rare earth elements indicates that the source materials of the study area are mainly from the felsic source in the upper crust. The elemental differentiation causes the Eu depletion in the upper crust and Eu enrichment in the lower crust. The uniform and gentle variations of HREEs can be explained by the lack of HREE differentiation in the upper crust. La/Yb-∑REE source rock identification proves that the sandstone source rocks in the study area are mainly felsic rocks of the upper crust and basaltic rocks, with mixed granite. According to REE distribution and La/Yb-∑REE source rock identification chart, gravity flows in the study area are related to the Archean in the northeastern and east margin of the basin and the maternal rocks of the metamorphic type in the Proterozoic era (Shi et al., 2007), indicating that the gravity-flow deposits in the study area are mainly supplied by provenance from the northeast.

5.4.3 Exploration of Triggering Mechanism

Paleoearthquakes of varying magnitude that occurred in the same depositional period can be proved by the liquefaction deformation at the interface of thin sand and mudstone (**Figure 7A**; **Table 8**), and it can also be proved by the fault lines resulted from tectonic movements (**Figure 7B**; **Table 8**). According to the method that judges earthquake magnitude using depositional structures, earthquakes with a magnitude of 4.5–5.5 are speculated to occur frequently in the southwestern Ordos Basin during the Late Triassic (Rodriguez-Pascua et al., 2000). The age of the tuffs interbedded in the sediments shows the relation between volcanic activity and active faulting (Zhang et al., 2014; Chen B. et al., 2019). Volcanic eruptions or tectonic faulting have caused multiple slides to develop in the southwestern sector and less in the northeastern part. In addition, thin tuffs (**Figures 7C,D**; **Table 8**) are commonly found in great cumulative thickness in northeast areas. The thickness of tuff deposits decreases from the southwest to the northeast of the basin (Yang and Deng, 2013; Fu et al., 2018), suggesting that the triggering of geological events contributed more to the deposits of gravity-flow in the southwest.

Laboratory simulations show that flood-type gravity flows are formed during the basin flooding stage, and they are thicker and have a higher content of argillaceous sand and coarse fraction than the gravity flows of slump genesis. Besides, a small number of reverse segments are visible (Cao et al., 2017; Li Z. et al., 2018). The single layer of sandy debris flow in the southwest is generally less than 2 m in thickness and is inter-deposited with thick mudstones. Relatively small amounts of gravel with a long axis of no more than 5 cm can be found. However, the sandy debris flows in the northeast are dominated by thick massive sand bodies with a single layer thicker than 5 m, which are overlapped in multiple phases longitudinally. The content of gravel is relatively high, and large mud gravels with a diameter exceeding 5 cm are frequently observed (**Figure 7F**; **Table 8**). Some massive chalk-fine sandstones feature negative grain sequence, (**Figure 4B**; **Table 6**), and a large number of fossilized plant fragments (**Figure 7E**; **Table 8**) and scouring surfaces (**Figure 7G**; **Table 8**) are visible. What is more, thin section observation reveals that feldspathic clastic sandstone dominates the rock in the southwest (**Figure 8A**), while clastic sandstone in the northeast (**Figure 8B**), with the former having a higher compositional maturity than the latter. Existing research also showed that the Sr/Cu value of trace elements in the Chang 6 of the Ordos Basin is less than 10. The Asseretospora-Walchiites sporulation assemblage shows that the flora is dominated by warm and wet-loving components, followed by hot and humid-loving components (Liu et al., 2015; Fu et al., 2018), reflecting a warm and humid climate. Extensive evidence indicates that gravity-flow deposits in the northeast have the shallow-water background and thick deposits, and they are formed in a periodically changing high-energy water environment. Lithological and geochemical evidence proves the frequent flooding in the northeast that continuously recharged shallow-water deposits to the lake basin, which is consistent with the provenance analysis. As a result, the gravity-flow in the northeast is considered to be spatially continuous thick layer of gravity-flow deposits formed thanks to seasonal floods that carry shallow-water deposits into the deep lake.

5.5 Depositional Model of Gravity Flow

The above analysis reveals that the study area mainly develops three flow types of gravity flow, namely, slide-slump, sandy debris flow, and turbidity flow. The sedimentological evidence indicates geological events such as volcanoes and earthquakes. The lake basin bottom shape, provenance supply, and triggering

FIGURE 7 | Core sign for triggering mechanism of gravity-flow in the study area.

TABLE 8 | The well name, depth, and phenomenon description of **Figure 7**. See **Figure 1** for the locations of wells.

Figure 3	Well name	Depth/m	Phenomenon description
A	Ning 25	1762.6–1762.7	Liquefaction and deformation of sandstone grain layers under seismic action
B	Bai 246	2056.8–2056.9	Four tuffs developed in the southwestern slip system, indicating multiple phases of volcanic activity during the depositional period
C	Ning 117	1,512.0–1,514.0	Slump deformation structure, micro-deformated convolute bedding
D	Ning 117	1,513.0–1,513.2	Lithologic interface tuff development indicative of volcanism
E	Yue 66	2012.3–2012.4	Gray fine sandstone with layers rich in fossilized plant fragments (dark portions)
F	Ling 79	1,647.5–1,647.6	Semi-consolidated dark mud gravels broken and torn during the earthquake and deposited *in situ* in angular form
G	Zhuang 42	1922.4–1922.5	Sandy debris flow with overlying mud interlayer with scouring surface

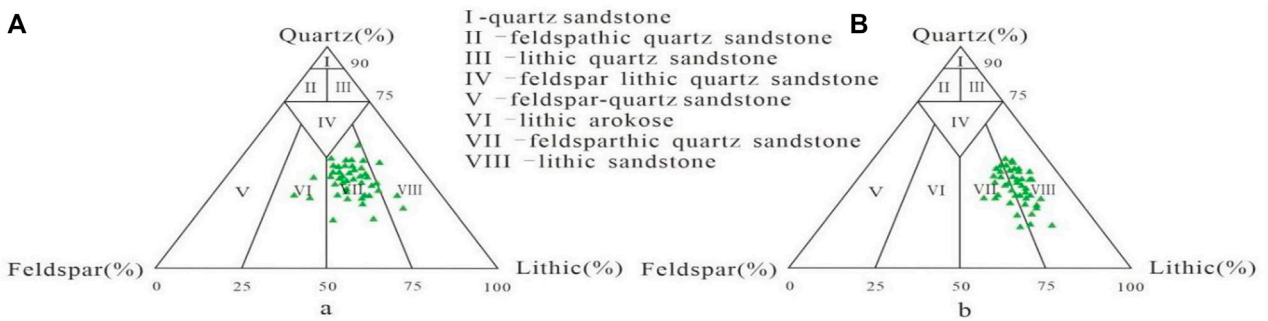

FIGURE 8 | Triangle for the classification of sandstones in different gravity-flow deposition models. **(A)** Triangle for the classification of sandstone in the southwest of the study area; **(B)** triangle for the classification of sandstone in northeast of the study area.

mechanisms obviously affect the distribution and formation of gravity flow.

The southwest Qinling has relatively insufficient supply, which is mostly driven by geological events such as volcanoes and earthquakes. Deposits bypass only because of the slope-fold zone at the bottom of the lake basin where slump turbidite develops. The well Ban29 in the southwest is selected as a typical well. The histogram shows the inter-deposition of thin siltstone or muddy siltstone and mudstone, as well as sedimentary structures such as wavy bedding, convolute bedding, deformation slump, and flame structures. All of them are considered to be triggered by geological events (**Figure 9A**, **Figure 2** for the location of well). The deposits remain temporarily at high places collapsed, sliding down along the slope-break zone. In addition, they undergo four evolutionary stages of sliding, slumping, debris flow, and turbidity current during the transition from proximal to distal sediments. Single-phase slump

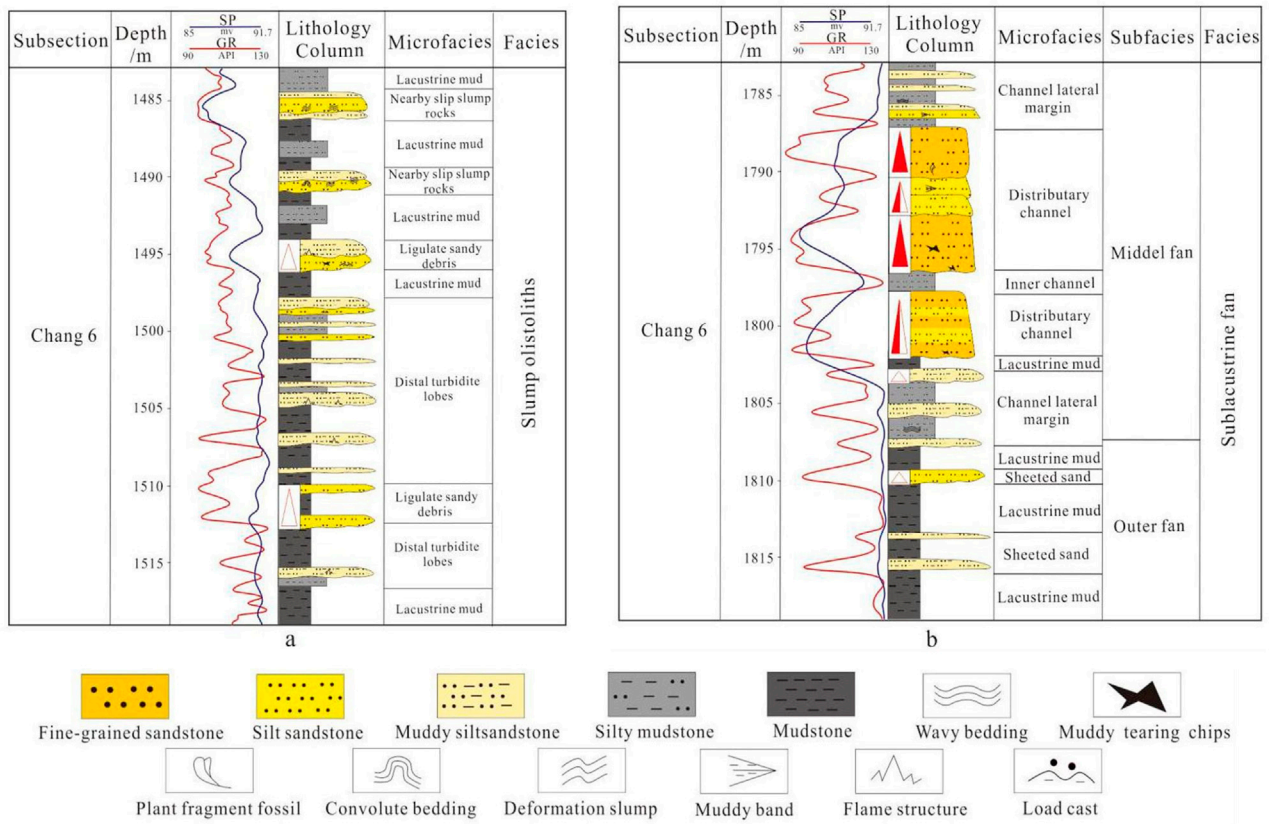

FIGURE 9 | Comprehensive map of lithology and depositional facies. See **Figure 2** for the location of wells. **(A)** Comprehensive map of lithology and depositional facies of well ban 29, slump olistoliths model. **(B)** Comprehensive map of lithology and depositional facies of well Zhuang 42, sublacustrine model.

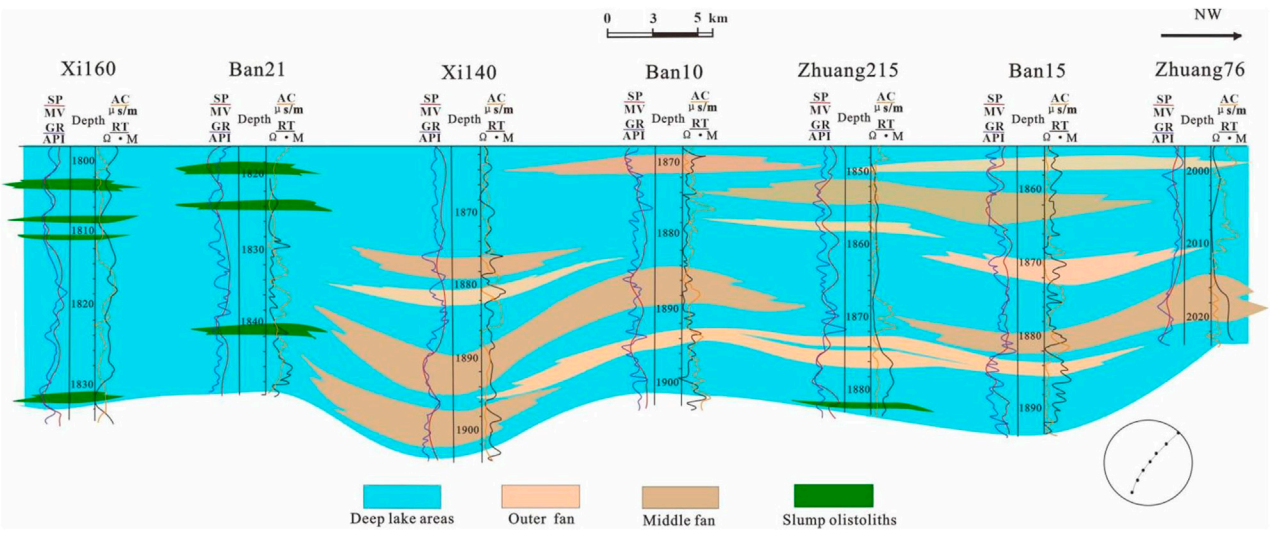

FIGURE 10 | Interwell sedimentary facies correlation. Well Xi160-well Ban21-well Xi140-well Ban10-well Zhuang215-well Ban15-well Zhuang76. See **Figure 2** for the location of the line of interwell correlation.

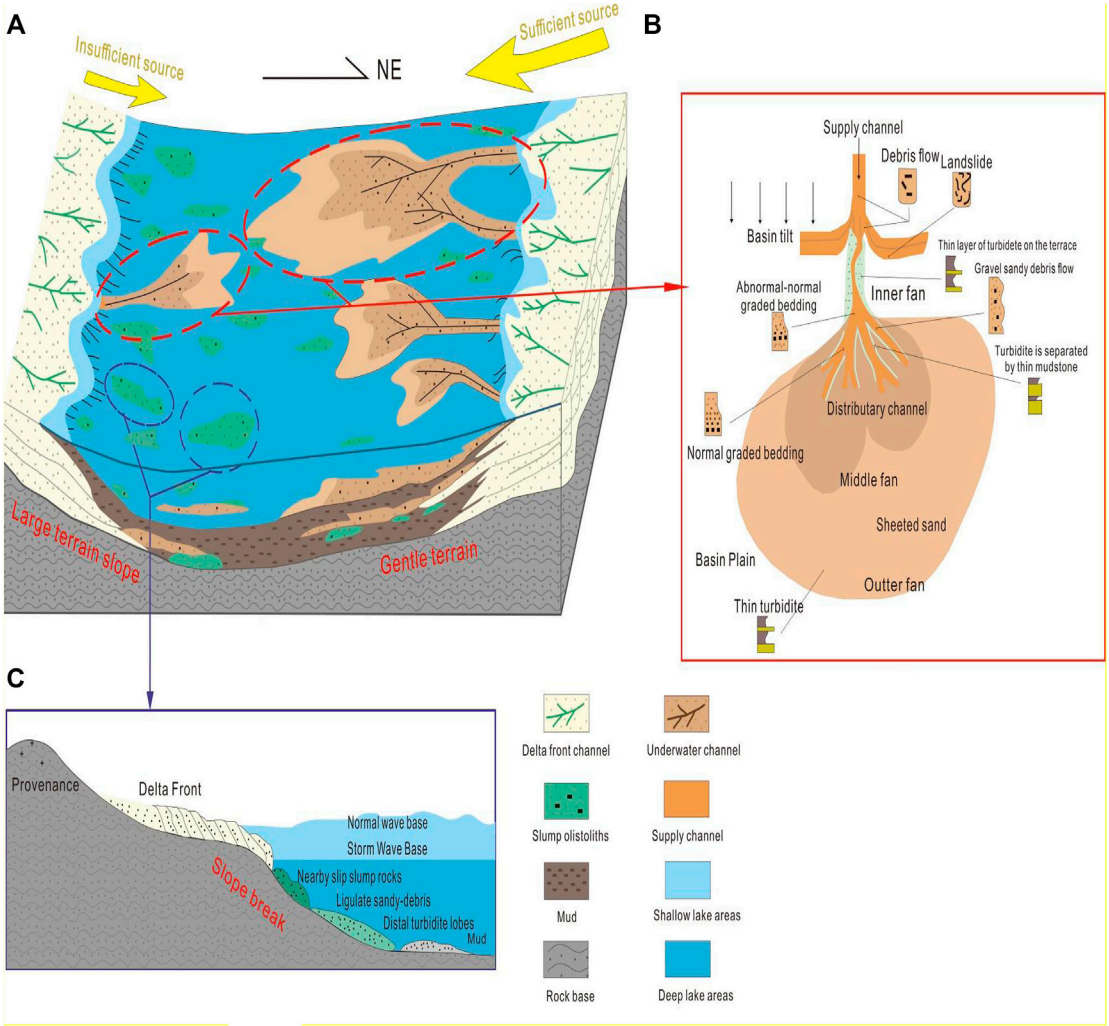

FIGURE 11 | Gravity-flow depositional model of Chang 6 in Heshui area. **(A)** Gravity depositional system in the study area; **(B)** depositional model of slump olistoliths; **(C)** depositional model of sublacustrine fans.

turbidite can be subdivided into three microfacies, including proximal slide-slump, debris flow lobe, and distal turbidite lobe based on flow transformation and spatial distribution (**Figure 10B**; **Figure 2** for the location of well).

Interwell correlation—well Xi160-well Ban21-well Xi140-well Ban10-well Zhuang215-well Ban15-well Zhuang76 is selected to compare the lateral distribution of sedimentary facies (**Figure 10**; see **Figure 2** for the location of the line of interwell correlation). The section is distributed in a northeast to southwest direction, parallel to the input direction of the outcrop. It is manifested by the development of sublacustrine fans in the northeast, with large thickness and good spatial continuity, and the long extension of sand bodies. The sedimentary slump-turbidite in the southwest is isolated and discontinuous, with shorter extensions.

The northeastern part that is well supplied with material resources has a wide and gentle bottom shape. The well Zhuang42 in northeast is selected as a typical well. From the histogram, it can be seen that multi-stage fine sandstone and siltstone are superimposed to form a huge, massive sand body. Muddy tearing chips or plant fragment fossil can be seen inside, and the load cast can be seen at the bottom (**Figure 9B**). Deposits accumulated on the front of the delta are transported by flood into the deep lake, forming a sublacustrine fan: a gravity-flow fan featuring watercourse (**Figure 11A**). During the rainy season, flood carries shallow-water deposits to the basin through the recharge channel. At the same time, high-density gravity-flow consisting of sand, mud, and gravel enters the semi-deep and deep lake, eroding the underlying unconsolidated soft deposits to form a lacustrine subaqueous channel (**Figure 11C**). As the slope of the basin decreases, the kinetic energy of the channel decreases, forming a longitudinally and horizontally interconnected braided channel (**Figure 11C**). In this channel, massive, homogeneous fine-siltstone is distributed inside and mud-rich tear debris at the top (**Figures 4F,G**). Evident scouring marks observed at the lithologic interface (**Figure 4H**) are typical sandy clastic flow deposits. The multi-phase braided channels are prone to superposition or interbedded with thin mudstone. On the flanks

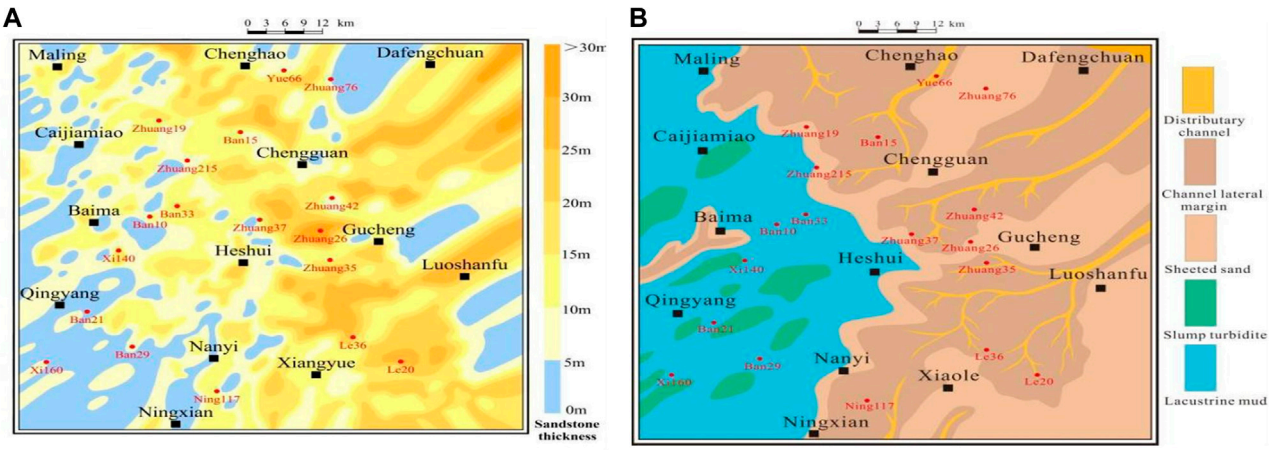

FIGURE 12 | The planar distributions of sand bodies and sedimentary facies are well correlated. **(A)** Plane distribution diagram of the sand body; **(B)** Plane distribution map of depositional facies.

of the channels, typical turbidites with Bouma sequences of B–E and C–E sections (**Figure 11C**) are formed, featuring the positive rhythmical progression of siltstone, muddy siltstone, and argillaceous siltstone with a thickness of less than 1 m. The microfacies are formed by the overflow of deposits in the braided channels. On entering the lake bottom plain, the erosion of gravity-flow on the overlying deposits weakens and the channels disappear, forming a wide area of sheet sand in outer fan architecture, which interbeds with semi-deep lacustrine-deep lacustrine mudstone. In these strata, sandy lens (**Figure 4M**) and sections C, D, and E of the Bouma sequences (**Figures 4K,L**) are visible in the core so they are typical turbidite deposits. According to lithological signatures and sand thickness, the gravity-flow in the northeastern part is controlled by the middle and outer sides of the sublacustrine fan, which can be further subdivided into four microfacies covering braided channel, channel flank wing, interchannel, and sheet sand.

5.6 Petroleum Geological Significance of Gravity-Flow Deposits

The southwestern part of the study area is dominated by slump turbidites sedimented by event collapse, forming disconnected sand bodies in the shape of an isolated island (**Figure 12A**). Statistically, the single-phase slump turbidites in the study area are no more than 2 m in thickness, and are extended within 15 km. They are also independent of each other (**Figure 12B**). As for the bottom shape with a certain slope drop angle, gravity-flow undergoes multiple flow transformations along the slope. The superstition and development of multi-stage slump lobes lead to the formation of a mixed event layer of sandy debris flow and turbidity current, i.e., fine-grained depositional rock interbedded with siltstone and mudstone. The sudden and rapid deposits of the event gravity-flow enable it to bury and preserve organic matter in a relatively short period, indirectly promoting hydrocarbon generation and expulsion. As a result, the fine-grained depositional rock developed from the fluid transformation in the slump turbidites is in a favorable position for hydrocarbon generation and enrichment. Besides, the brittle minerals of terrestrial origin are abundant in this area, including quartz, feldspar, and calcite, determining the fracturing parameters in the development of unconventional petroleum, and serving as a potential "sweet spot" for deep-water tight oil and gas.

Flood-forming sublacustrine fans are widely developed in the northeastern part of the study area. Multiple sublacustrine fans may be stimulated simultaneously in the temporary sediment retention areas at the gentle slope of the delta front by multi-stage floods, and the superposition of multi-phase fans controls the distribution range of contiguous sand bodies in the study area (**Figures 12A,B**). The thickness ranged from 1.8 to 13.7 m for the sandy debris flow with better-sorting properties in the middle fan braided channel microfacies, with the average being 7.6 m. The sheet sand in the outer fan is turbidite sediment transformed by the liquefaction and dilution of sandy debris flow. The physical property of argillaceous siltstone and muddy siltstone between multi-phase fans becomes poor in the burial evolution given the strong compaction and recrystallization of the heterogeneous base, forming favorable caprock and plugging zone. The thick sand body of sandy debris flows genesis in the middle fan, and the sheet sand of current turbidity genesis in the outer fan can be employed as transport and reservoir layers. Under the microscope, the intergranular pores remaining between terrestrial clastic particles such as quartz and feldspar can be seen (**Figures 13A–C**). During the diagenesis stage, the feldspar is easily dissolved to form solution expansion pores (**Figure 13D**) or intragranular dissolved pores (**Figure 13E**). In addition, due to tectonic action, structural fractures are easily formed in brittle mineral-rich rocks (**Figure 13F**), providing effective space for oil and gas storage. The periodicity of sedimentation explains the variability of the rock-forming evolution process, which controls the formation of deep-water lithological traps and hydrocarbon enrichment under deep burial conditions. On the other hand, floods transport a large amount of organic matter from terrestrial sources and shallow waters, and the enrichment of organic matter changes the original ecological environment of the basin and

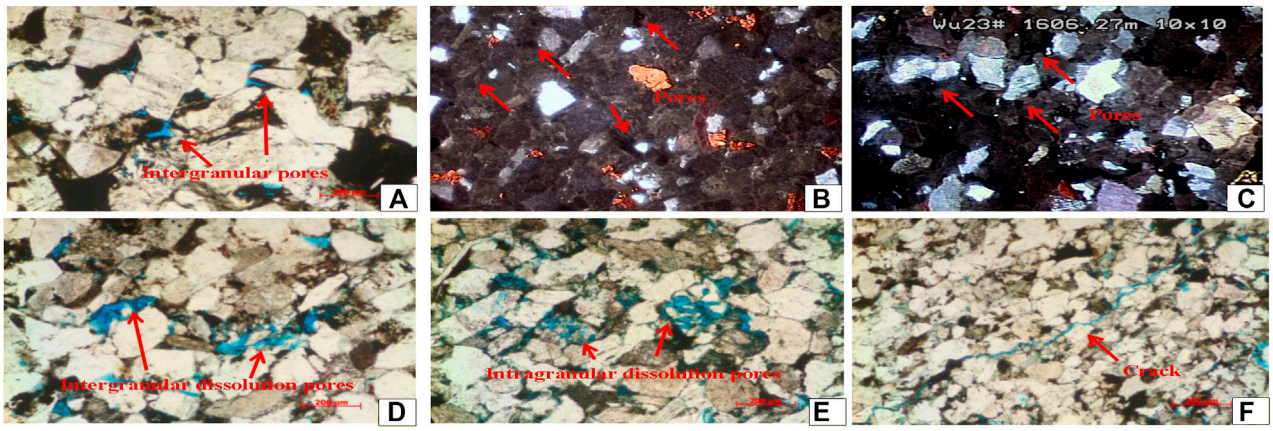

FIGURE 13 | Reservoir space caused by gravity flow under microscope and cathodoluminescence. See **Figure 2** for the location of wells. **(A)** Residual intergranular pores can be seen among the quartz grains, well Cai12, depth 2000.8 m; **(B)** Cathodoluminescence; visible calcite (orange, yellow) and dolomite (orange) cementation; clastics are interlocked; and pores are not luminescence. Well Zhuang70, depth 1735.35 m; **(C)** Cathodoluminescence; fine-grained feldspar sandstone; feldspar content between 55–60%. Well Wu23, depth 1,606.27 m; **(D)** Intergranular dissolution reaming is developed. Well Li183, depth 2068.3 m; **(E)** Intragranular dissolution pores of feldspar are developed. Well Li183, depth 2,105.8 m; **(F)** Structural micro-cracks. Well Li312 , depth 2087.6 m.

promotes the survival and reproduction of microorganisms, which directly or indirectly increases the content of organic carbon (Khripounoff et al., 2009; Yuan et al., 2015) and improves the hydrocarbon generation potential.

6 CONCLUSION

1) For semi-deep and deep lakes, gravity-flow deposits are extensively developed in the Chang 6 oil group in the Heshui area of Ordos Basin. Three types of gravity flow are identified, namely, slide-slump, sandy debris flow, and turbidity current. In addition, two depositional models of gravity flow are observed, i.e., slump turbidite and sublacustrine fan.
2) Driven by gravity, gravity-flow transports along the slope and undergoes fluid transformation with the participation of surrounding water. The transformation from slide-slump to sandy debris flow is subject to fragmentation and liquefaction, while that from sandy debris flow to turbidity current tends to be influenced by liquefaction and fluid mixing. The flow transformation of multi-phase gravity-flow results in the spatial superposition of different types of gravity flow, causing the interdeposition of multiple rock types and facilitating the generation and storage of oil and gas.
3) Sublacustrine fans of flood origin are extensively developed in the northeastern part of the study area. Besides, the superposition of multi-phase fans controls the distribution of contiguous sand bodies. In the middle fan-braided channel microfacies, the sandy debris flow with favorable sortability mainly leads to the formation of thick massive sand bodies. In the southwestern part of the study area, slump turbidites are sedimented by event collapse dominate, causing the formation of isolated disconnected sand bodies, and serving as a potential "sweet spot" for the development of deep-water tight oil and gas.

DATA AVAILABILITY STATEMENT

The original contributions presented in the study are included in the article/Supplementary Material. Further inquiries can be directed to the corresponding author.

AUTHOR CONTRIBUTIONS

All authors listed have made a substantial, direct, and intellectual contribution to the work and approved it for publication.

ACKNOWLEDGMENTS

This study was funded by the National Science and Technology Major Project of China (2016ZX05050006). We also thank the State Key Laboratory of Oil and Gas Reservoir Geology and Exploration of Chengdu University of Technology and Xi'an Shiyou University for providing samples and data, and for permission to publish this work.

REFERENCES

Amy, L., Talling, P., Peakall, J., Wynn, R., and Thynne, R. (2005). Bed Geometry Used to Test Recognition Criteria of Turbidites and (sandy) Debrites. *Sed Geol.* 179 (1-2), 163–174. doi:10.1016/j.sedgeo.2005.04.007

Bell, D., Kane, I. A., Pontén, A. S. M., Flint, S. S., Hodgson, D. M., and Barrett, B. J. (2018). Spatial Variability in Depositional Reservoir Quality of Deep-Water Channel-Fill and Lobe Deposits. *Mar. Pet. Geology.* 98, 97–115. doi:10.1016/j.marpetgeo.2018.07.023

Bernhardt, A., Stright, L., and Lowe, D. R. (2012). Channelized Debris-flow Deposits and Their Impact on Turbidity Currents: The Puchkirchen Axial

Channel belt in the Austrian Molasse Basin. *Sedimentology* 59, 2042–2070. doi:10.1111/j.1365-3091.2012.01334.x

Bouma, A. H. (1962). *Sedimentology of Some Flysch Deposits: A Graphic Approach to Facies Interpretation*. Amsterdam: Elsevier, 217–222.

Cao, Y., Wang, S., Wang, Y., Yang, T., Zhang, S., and Zhang, H. (2017). Sedimentary Characteristics and Depositional Model of Slumping Deep-Water Gravity Flow Deposits: A Case Study from the Middle Member 3 of Paleogene Shahejie Formation in Linnan Subsag, Bohai Bay Basi. *J. Palaeogeog.* 19 (3), 419–432. doi:10.7605/gdlxb.2017.03.032

Chen, B., Lin, C., Ma, C., Ren, L., Wang, J., Li, Z., et al. (2019b). Types, Characteristics and Sedimentary Model of Deep- Water Gravity Flow Deposition in the Steep Slope Zone of Terrestrial Faulted Lacustrine basin : a Case Study of the Es_4^S Submember in the Shengtuo Area of Dongying Depression. *Acta Geol. Sin* 93 (1), 2921–2932. doi:10.19762/j.cnki.dizhixuebao.2019098

Chen, C., Chen, X., Huang, J., Shi, Y., Shi, Y ., Zhu, Y., et al. (2019a). Relationship between Orogenic belt Uplift and Non-equilibrium Subsidence Basins: a Case Study of Chang 7 and Chang 6 Oil Reservoirs in Longdong Area, Ordos Basin. *Petrol. Geol. Exper.* 41 (5), 674–681. doi:10.11781/sysydz201905674

Covault, J. A., Kostic, S., Paull, C. K., Ryan, H. F., and Fildani, A. (2014). Submarine Channel Initiation, Filling and Maintenance from Sea-Floor Geomorphology and Morphodynamic Modelling of Cyclic Steps. *Sedimentology* 61 (4), 1031–1054. doi:10.1111/sed.12084

Du, J. (2015). Characteristics of Gravity Flow Sediment and its Geologic Significance in Northern Songliao Basin. *Acta Sedimentol. Sin.* 33 (3), 385–393. doi:10.14027/j.cnki.cjxb.2015.02.018

Fic, J., and Pedersen, P. K. (2013). Reservoir Characterization of a "Tight" Oil Reservoir, the Middle Jurassic Upper Shaunavon Member in the Whitemud and Eastbrook Pools, SW Saskatchewan. *Mar. Pet. Geology.* 44, 41–59. doi:10.1016/j.marpetgeo.2013.03.013

Fu, J., Li, S., Xu, L., and Niu, X. (2018). Paleo-sedimentary Environmental Restoration and its Significance of Chang 7 Member of Triassic Yanchang Formation in Ordos Basin, NW China. *Pet. Explor. Dev.* 45 (6), 936–946. doi:10.1016/s1876-3804(18)30104-6

Fu, Q., Lv, M., and Liu, Y. (2008). Developmental Characteristics of Turbidite and its Implication on Petroleum Geology in Late-Triassic Ordos Basin. *Acta Sedimentol. Sin.* 26 (2), 186–192. doi:10.14027/j.cnki.cjxb.2008.02.003

Fu, S., Deng, X., and Pang, J. (2010). Characteristics and Mechanism of Thick Sandbody of Yanchang Formation at the Centre of Ordos Basin. *Acta Sedimentol. Sin.* 28 (6), 1091–1098. doi:10.14027/j.cnki.cjxb.2010.06.012

Ghanizadeh, A., Clarkson, C. R., Aquino, S., Ardakani, O. H., and Sanei, H. (2015). Petrophysical and Geomechanical Characteristics of Canadian Tight Oil and Liquid-Rich Gas Reservoirs: I. Pore Network and Permeability Characterization. *Fuel* 153 (1), 664–681. doi:10.1016/j.fuel.2015.03.020

Haughton, P., Davis, C., McCaffrey, W., and Barker, S. (2009). Hybrid Sediment Gravity Flow Deposits - Classification, Origin and Significance. *Mar. Pet. Geology.* 26 (10), 1900–1918. doi:10.1016/j.marpetgeo.2009.02.012

Khripounoff, A., Vangriesheim, A., Crassous, P., and Etoublean, J. (2009). High Frequency of Sediment Gravity Flow Events in the Var Submarine canyon (Mediterranean Sea). *Mar. Geology.* 263 (1-4), 1–6. doi:10.1016/j.margeo.2009.03.014

Kuenen, P. H., and Migliorini, C. I. (1950). Turbidity Currents as a Cause of Graded Bedding. *J. Geology.* 58 (2), 91–127. doi:10.1086/625710

Kvale, E. P., Flenthrope, C., and Mace, C. (2017). Carbonate-Dominated Hybrid Sediment Gravity Flows Within the Upper Wolfcamp, Delaware Basin, USA: Vectors for Transmitting Terrestrial Organics into a Deep Marine Basin. *AAPG Search Discov.*, 10956.

Li, W., Pang, J., Cao, H., Xiao, L., and Wang, R. (2009). Depositional System and Paleogeographic Evolution of the Late Triassic Yanchang Stage in Ordos Basin. *J. Northwest. Univ.* 39, 501–506. doi:10.16152/j.cnki.xdxbzr.2009.03.011

Li, X., Chen, Q., Liu, H., Wan, Y., and Wei, L . (2011). Features of sandy Debris Flows of the Yanchang Formation in the Ordos basin and its Oil and Gas Exploration Significance. *Acta Sedimentol. Sin.* 85 (5), 223–238. doi:10.1111/j.1755-6724.2011.00550.x

Li, X., Liu, H., Pan, S., Chen, Q., WanYan, R., Xu, W., et al. (2018a). Subaqueous sandy Mass-Transport Deposits in Lacustrine Facies of the Upper Triassic Yanchang Formation, Ordos Basin, Central China. *Mar. Pet. Geology.* 97, 66–77. doi:10.1016/j.marpetgeo.2018.06.019

Li, Z., Wu, S., Xia, D., He, S., and Zhang, X. (2018b). An Investigation into Pore Structure and Petrophysical Property in Tight Sandstones: a Case of the Yanchang Formation in the Southern Ordos Basin, China. *Mar. Pet. Geology.* 97, 390–406. doi:10.1016/j.marpetgeo.2018.07.014

Liu, F., Zhu, X., Li, Y., Xu, L., Niu, X., Zhu, S., et al. (2015). Sedimentary Characteristics and Facies Model of Gravity Flow Deposits of Late Triassic Yanchang Formation in Southwestern Ordos Basin, NW China. *Pet. Exploration Dev.* 42 (5), 633–645. doi:10.1016/s1876-3804(15)30058-6

Liu, S., Ruan, Z., Yang, Z., Wu, Y., Li, Y., and Han, S. (2019). Provenance Evolution of Southern Margin of Ordos Basin during the Middle-Later Triassic and its Geological Implication. *J. Palaeogeog.* 21 (6), 939–358. doi:10.7605/gdlxb.2019.06.064

Liu, X.-X., Ding, X.-Q., Zhang, S.-N., and He, H. (2017). Origin and Depositional Model of Deep-Water Lacustrine sandstone Deposits in the 7th and 6th Members of the Yanchang Formation (Late Triassic), Binchang Area, Ordos basin, china. *Pet. Sci.* 14, 24–36. doi:10.1007/s12182-016-0146-x

Lowe, D. R. (1982). Sediment Gravity Flows: II. Depositional Model with Special Reference to the Deposits of High-Density Turbidity Currents. *J. Sediment. Res.* 52 (1), 279–297.

Luo, J., Li, J., Yang, B., Dai, Y., Li, B., Han, Y., et al. (2007). Provenance for the Chang 6 and Chang 8 Member of the Yanchang Formation in the Xifeng Area and in the Periphery Ordos Basin: Evidence from Petrologic Geochemistry. *Sci. China Ser. D-earth Sci.* 50, 75–90. doi:10.1007/s11430-007-6015-0

Ma, B., Cao, Y., Eriksson, K. A., Jia, Y., and Gill, B. C. (2017). Depositional and Diagenetic Controls on Deeply-Buried Eocene Sublacustrine Fan Reservoirs in the Dongying Depression, Bohai Bay Basin, China. *Mar. Pet. Geology.* 82, 297–317. doi:10.1016/j.marpetgeo.2017.02.014

Mchargue, T., Pyrcz, M. J., Sullivan, M. D., Clark, J. D., Fildani, A., Romans, B. W., et al. (2011). Architecture of Turbidite Channel Systems on the continental Slope: Patterns and Predictions. *Mar. Pet. Geology.* 28 (3), 728–743. doi:10.1016/j.marpetgeo.2010.07.008

Mulder, T., and Alexander, J. (2001). The Physical Character of Subaqueous Sedimentary Density Flows and Their Deposits. *Sedimentology* 48 (2), 269–299. doi:10.1046/j.1365-3091.2001.00360.x

Mulder, T. (2009). Marine Hyperpycnal Flows: Initiation, Behavior and Related Deposits. A Review. *Mar. Pet. Geol.* 20 (6-8), 861–882. doi:10.1016/j.marpetgeo.2003.01.003

Pan, S., Liu, H., Zavala, C., Liu, C., Liang, S., and Zhang, Q. (2017). Sublacustrine Hyperpycnal Channel-Fan System in a Large Depression basin: A Case Study of Nen 1 Member, Cretaceous Nenjiang Formation in the Songliao Basin, NE China. *Pet. Explor. Dev.* 44 (6), 860–870. doi:10.1016/s1876-3804(17)30103-9

Perry, S. E., Walls, J. D., and Ride, T. (2017). "Comparing and Contrasting Analytically Quantified Porosity and Pore Size Distributions in the Wolfcamp Formation from SEM Imaging, Nuclear Magnetic Resonance (NMR), and Crushed Rock Core Analysis," in Nuclear Magnetic Resonance (NMR), and Crushed Rock Core Analysis, AAPG Annual Conference and Exhibition, Houston, TX.

Pu, X., Zhou, L., Han, W., Chen, C., Yuan, X., Lin, C., et al. (2014). Gravity Flow Sedimentation and Tight Oil Exploration in Lower First Member of Shahejie Formation in Slope Area of Qikou Sag, Bohai bay basin. *Pet. Exploration Dev.* 41 (2), 153–164. doi:10.1016/s1876-3804(14)60018-5

Qiao, B., Zhang, C., Li, S., Du, J., and Zhu, R. (2013). Feature of Gravity Flow deposit of the Zhuhai and Zhujiang Formations of Cenozoic in Huizhou Area, Pearl River Mouth Basin. *J. Palaeogeog.* 15 (1), 69–75. doi:10.7605/gdlxb.2013.01.007

Ran, Y., and Zhou, X. (2019). Sedimentary Characteristics and Petroleum Geological Significance of the Chang6 Gravity Flow in the Southwest Ordos Basin. *Acta Sedimentol. Sin.* 38 (3), 571–579. doi:10.14027/j.issn.1000-0550.2019.056

Rodríguez-Pascua, M. A., Calvo, J. P., De Vicente, G., and Gómez-Gras, D. (2000). Soft-sediment Deformation Structures Interpreted as Seismites in Lacustrine Sediments of the Prebetic Zone, Se spain, and Their Potential Use as Indicators of Earthquake Magnitudes during the Late Miocene. *Sediment. Geol.* 135 (1), 117–135.

Shanmugam, G. (2000). 50 Years of the Turbidite Paradigm (1950s-1990s): Deep-Water Processes and Facies Models-A Critical Perspective. *Mar. Pet. Geology.* 17 (2), 285–342. doi:10.1016/s0264-8172(99)00011-2

Shanmugam, G. (2013). New Perspectives on Deep-Water Sandstones: Implications. *Pet. Exploration Dev.* 40, 316–324. doi:10.1016/s1876-3804(13)60038-5

Shanmugam, G. (2016). Submarine Fans: a Critical Retrospective (1950-2015). *J. Palaeogeogr.* 5 (2), 110–184. doi:10.1016/j.jop.2015.08.011

Shanmugam, G. (1997). The Bouma Sequence and the Turbidite Mind Set. *Earth-Science Rev.* 42 (4), 201–229. doi:10.1016/s0012-8252(97)81858-2

Shi, C., Yan, M., and Chi, Q. (2007). Abundances of Chemical Elements of Granitoids in Different Geotectonic Units of China and Their Characteristics. *Acta Geol. Sin* 81 (1), 47–59. doi:10.1016/j.gsf.2011.02.002

Sonnenberg, A. S. (2017). The Giant Continuous Oil Accumulation in the Bakken Petroleum System, Williston Basin. *AAPG Search Discov.* 1-10. doi:10.1306/13572002M113508

Stevenson, C. J., and Peakall, J. (2010). Effects of Topography on Lofting Gravity Flows: Implications for the Deposition of Deep-Water Massive Sands. *Mar. Pet. Geology.* 27 (7), 1366–1378. doi:10.1016/j.marpetgeo.2010.03.010

Talling, P. J., Malgesini, G., and Felletti, F. (2012a). Can Liquefied Debris Flows deposit Clean Sand over Large Areas of Sea Floor? Field Evidence from the Marnoso-Arenacea Formation, Italian Apennines. *Sedimentology* 60 (3), 720–762. doi:10.1111/j.1365-3091.2012.01358.x

Talling, P. J., Masson, D. G., Sumner, E. J., and Malgesini, G. (2012b). Subaqueous Sediment Density Flows: Depositional Processes and deposit Types. *Sedimentology* 59 (7), 1937–2003. doi:10.1111/j.1365-3091.2012.01353.x

Wang, W., Jiang, Y., Swennen, R., Yuan, J., Liu, J., and Zhang, S. (2018). Pore-throat Characteristics of Tight sandstone Reservoirs Composed of Gravity Flow Sediments: Yingcheng Formation, Longfengshan Sag, China. *J. Pet. Sci. Eng.* 171, 646–661. doi:10.1016/j.petrol.2018.07.024

Xian, B., Wang, J., Gong, C., Yin, Y., Chao, C., Liu, J., et al. (2018). Classification and Sedimentary Characteristics of Lacustrine Hyperpycnal Channels: Triassic Outcrops in the South Ordos Basin, central China. *Sediment. Geology.* 368, 68–82. doi:10.1016/j.sedgeo.2018.03.006

Xu, Q., Shi, W., Xie, X., Manger, W., McGuire, P., Zhang, X., et al. (2016). Deep-lacustrine sandy Debrites and Turbidites in the Lower Triassic Yanchang Formation, Southeast Ordos Basin, central China: Facies Distribution and Reservoir Quality. *Mar. Pet. Geology.* 77, 1095–1107. doi:10.1016/j.marpetgeo.2016.08.011

Yang, H., and Deng, X. (2013). Deposition of Yanchang Formation Deep-Water sandstone under the Control of Tectonic Events, Ordos Basin. *Pet. Explor. Dev.* 40 (5), 513–520. doi:10.1016/s1876-3804(13)60072-5

Yang, H., Niu, X., Luo, S., Feng, S., and Lv, Q. (2015). Research of Simulated experiment on Gravity Flow Deposits of Tight Sand Bodies of Chang 7 Formation in Longdong Area, Ordos Basin. *Earth Sci. Front.* 22 (3), 322–332. doi:10.13745/j.esf.2015.03.028

Yang, R., He, Z., Qiu, G., Jin, Z., Sun, D., and Jin, X. (2014). Late Triassic Gravity Flow Depositional Systems in the Southern Ordos Basin. *Pet. Explor. Dev.* 41 (6), 661–670. doi:10.1016/s1876-3804(14)60086-0

Yang, T., Cao, Y., and Tian, J. (2020). Discussion on Research of Deep-Water Gravity Flow Deposition in Lacustrine basin. *Acta Sedimentol. Sin.* 39 (1), 88–111. doi:10.14027/j.issn.1000-0550.2020.037

Yao, J., Deng, X., Zhao, Y., Han, T., Chu, M., and Pang, J. (2013). Characteristics of Tight Oil in Triassic Yanchang Formation, Ordos Basin. *Pet. Exploration Dev.* 40 (2), 161–169. doi:10.1016/s1876-3804(13)60019-1

Yu, J., Yang, Y., and Du, J. (2010). Sedimentation during the Transgression Period in Late Triassic Yanchang Formation, Ordos Basin. *Pet. Explor. Dev.* 37 (2), 181–187.

Yuan, X., Lin, S., Liu, Q., Yao, J., Wang, L., Guo, H., et al. (2015). Lacustrine fine-grained Sedimentary Features and Organicrich Shale Distribution Pattern: A Case Study of Chang 7 Member of Triassic Yanchang Formation in Ordos Basin, NW China. *Pet. Exploration Dev.* 42 (1), 37–47. doi:10.1016/s1876-3804(15)60004-0

Zhang, H., Peng, P., and Zhang, W. (2014). Zircon U-Pb Ages and Hf Isotope Characterization and Their Geological Significance of Chang 7 Tuff of Yanchang Formation in Ordos Basin. *Acta Pet. Sinica* 30 (2), 565–575.

Zhang, K. (1989). *Block Structure and Resources in Ordos Basin*. Shanxi: Shanxi Science and Technology Press.

Zhang, Z., Chen, S., Yang, H., Fu, J., Yao, J., Yu, J., et al. (2016). Retracted: Tight Oil Accumulation Mechanisms of Triassic Yanchang Formation Chang 7 Member, Ordos Basin, China. *Pet. Exploration Dev.* 43 (4), 644–654. doi:10.1016/s1876-3804(16)30075-1

Zhao, W.-z., Wang, Z.-c., Wang, H.-j., and Wang, Z.-y. (2008). Principal Characteristics and Forming Conditions for Medium-Low Abundance Large Scale Oil/gas fields in china. *Pet. Exploration Dev.* 35 (6), 641–650. doi:10.1016/s1876-3804(09)60097-5

Z. He (Editor) (2003). *Evolution of Ordos Basin and Oil and Gas* (Beijing: Petroleum Industry Press.), 95–105.

Zou, C., Wang, L., Li, Y., Tao, S., and Hou, L. (2012). Deep-lacustrine Transformation of sandy Debrites into Turbidites, Upper Triassic, Central China. *Sediment. Geology.* 265-266 (Jul. 15), 143–155. doi:10.1016/j.sedgeo.2012.04.004

Zou, C., Zhao, Z., Yang, H., Fu, J., Zhu, R., and Yuan, X. (2009). Genetic Mechanism and Distribution of Sandy Debris Flows in Terrestrial Lacustrine Basin. *Acta Sedimentol. Sin.* 27 (6), 1065–1075. doi:10.14027/j.cnki.cjxb.2009.06.022

Conflict of Interest: The authors declare that the research was conducted in the absence of any commercial or financial relationships that could be construed as a potential conflict of interest.

Publisher's Note: All claims expressed in this article are solely those of the authors and do not necessarily represent those of their affiliated organizations, or those of the publisher, the editors and the reviewers. Any product that may be evaluated in this article, or claim that may be made by its manufacturer, is not guaranteed or endorsed by the publisher.